

The University of California San Francisco, Brain Metastases Stereotactic Radiosurgery (UCSF-BMSR) MRI Dataset

Jeffrey D. Rudie MD PhD^{1,2}, Rachit Saluja MSE³, David A. Weiss MSE¹, Pierre Nedelec MS¹, Evan Calabrese MD PhD^{1,4}, John B. Colby MD PhD¹, Benjamin Laguna MD¹, John Mongan MD PhD¹, Steve Braunstein MD PhD⁴, Christopher P. Hess MD PhD¹, Andreas M. Rauschecker MD PhD¹, Leo P. Sugrue MD PhD¹, Javier E. Villanueva-Meyer MD¹

1. University of California San Francisco, Department of Radiology & Biomedical Imaging
2. University of California, San Diego, Department of Radiology
3. University of Pennsylvania, Department of Radiology
4. Duke University, Department of Radiology
5. University of California San Francisco, Department of Radiation Oncology

Corresponding Author

Jeff Rudie, MD, PhD

Jeff.Rudie@gmail.com

Abstract

The University of California San Francisco Brain Metastases Stereotactic Radiosurgery (UCSF-BMSR) dataset is a public, clinical, multimodal brain MRI dataset consisting of 560 brain MRIs from 412 patients with expert annotations of 5136 brain metastases. Data consists of registered and skull stripped T1 post-contrast, T1 pre-contrast, FLAIR and subtraction (T1 pre-contrast - T1 post-contrast) images and voxelwise segmentations of enhancing brain metastases in NifTI format. The dataset also includes patient demographics, surgical status and primary cancer types. The UCSF-BSMR has been made publicly available in the hopes that researchers will use these data to push the boundaries of AI applications for brain metastases.

Introduction

Public datasets, such as those made available through the cancer imaging archive (TCIA; (1)) and the multimodal brain tumor segmentation challenge (BraTS; (2)) have been critical in supporting advances in the field of biomedical image segmentation in neuro-oncology, particularly in glioma. Brain metastases are the most common central nervous system tumor (3,4) and new effective treatment methods have led to a dramatic rise in imaging for their detection (5). Detection of very small metastases remains a challenge (6–8), yet there is little publicly available data to address this problem (6).

Here we present the University of California, San Francisco Brain Metastases Stereotactic Radiosurgery (UCSF-BMSR) MRI Dataset. This dataset contains 560 multimodal brain MRIs from 412 patients undergoing gamma knife radiosurgery with expert annotations of brain metastases. There are annotations of 5136 brain metastases, including two sets of annotations in 99 cases. We also provide a current benchmark of metastasis detection and segmentation performance in this dataset using the nnU-Net (9).

Materials and Methods

Patient Population

The dataset consists of 560 brain MRIs from 412 patients (61 ± 12 years, 238 women; Table 1) who were undergoing stereotactic radiosurgery planning at the University of California, San Francisco medical center. MRIs were identified through a search of institutional radiology archives (mPower, Nuance Communications, Inc) of stereotactic radiosurgery studies performed between January 1st 2017 and February 29th, 2020. This dataset overlaps with a prior study (8), which contains additional details of the inclusion/exclusion criteria. Three exams included in the prior study (8), were not included in this dataset given missing FLAIR sequence. Prior craniotomies for resections or biopsies are present in 135 of the scans.

Imaging Data Acquisition

Images were first converted from DICOM into Nifti format using dcm2nii. The T1-weighted spoiled gradient-echo (T1), T1 post-contrast (T1-post) images, and T2 fluid-attenuation inversion recovery (FLAIR) are included for each scan. The majority (373 of 560) of studies were acquired on a 1.5 Tesla GE SignaHDxt scanner. 149 studies were acquired on a 1.5 Tesla Philips Achieva scanner and 38 were acquired on a 3.0 Tesla GE Discovery MR750. Additional details of the scan parameters can be found elsewhere (8).

Brain Metastases Annotations

Reference standard brain metastasis voxelwise segmentations were created using ITK-SNAP (10); <http://www.itksnap.org/>) by a neuroradiology fellow (JDR, BL) or attending neuroradiologist (LPS and JEV, with 5 and 4 years of experience as neuroradiology attending

physicians) with the final radiology report used as a reference. The T1, T1-post, and subtraction images were available to guide the manual segmentations. Only the enhancing portions of the metastases were segmented. Areas of central necrosis and areas of T1 intrinsic hyperintensity were not included in the segmentation masks. In cases with resection cavities, the nodular enhancing portion of the resection cavities were included in the segmentation masks. Ninety nine of the cases, representing unique subjects previously used as the test cases in (8), were segmented by two different neuroradiologists (one neuroradiology fellow (JDR) and one of two neuroradiology attendings (LPS and JEV) without reference to the final radiology report. Final reference standard segmentations for these cases were generated by combining and refining the two segmentations with reference to the final radiology report.

Image Pre-Processing

The T1 images were registered to the T1-post images by rigid registration (6 degrees of freedom). Subtraction images were generated by subtracting the registered T1 from T1-post images. For the purposes of protecting personal health information all images were skull stripped using a custom skull stripping network.

nnU-Net Convolutional Neural Network Experiments

In order to evaluate current, state-of-the-art, performance of metastasis segmentation and detection, we performed several experiments utilizing the nnU-Net (9) a 3D fully-convolutional network (3D Res-U-Net), a self-configuring method that performs pre-processing, network architecture and hyperparameter tuning. We evaluated different multichannel input combinations of the T1, T1-post, subtraction, and FLAIR images, a larger batch size (batch size of 6 rather

than default of 2), pretraining the network on the BraTS 2021 training dataset for enhancing tumor (n=1251), and the nnU-net modifications used by the winners of the BraTS 2021 challenge (2,11), which included group normalization and a larger network size. We also evaluated performance with different training sample sizes. Performance was evaluated in the 99 test cases for each of these experiments. In all experiments, the patch size was auto selected to be 64x192x160 and training was performed on a RTX 3090 GPU (CUDA version 11.2; NVIDIA corporation, Santa Clara, CA; 24 GB memory) for 1000 epochs using a combination of cross entropy and Dice loss function (1:1). We also calculated performance metrics between the two expert segmentations in 99 test cases relative to each other and relative to the final gold standard segmentations.

Results

Size and Distribution of Brain Metastases

Table 1 provides an overview of patient characteristics and metastasis number and size distribution, with details for each case provided in **Table S1**. The most common types of primary cancers were lung, breast, and melanoma. A total of 5136 brain metastases were segmented in the 560 MRIs with a mean of 9.2 ± 12.9 metastases and a median of 5 (IQR 2-11). The mean and median total metastasis volumes per MRI were $5.3 \pm 6.9 \text{ cm}^3$ and 2.6 cm^3 (IQR 0.6-6.9 cm^3). The mean and median individual metastasis volumes were $0.57 \pm 2.1 \text{ cm}^3$ and 0.05 cm^3 (IQR 0.02-0.18 cm^3). The distribution of metastases per scan and metastasis volumes are shown in **Figure 1**.

Performance of nnU-Net and Radiologist Segmentations

Table 2 provides the segmentation performance for the experiments detailed in the methods section within the test set (mean and median Dice, overall sample and average sample sensitivity, precision and F1 scores (Lesion wise Dice)). While there were minimal differences between different multichannel inputs, the model with T1, T1-post and subtraction images had the highest overall sensitivity (82.91%), so it was used for the remaining experiments. The additional modifications did not significantly alter performance, noting that the winning BraTS 2021 modifications (11) did have the highest overall F1 score and the model pretrained on BraTS 2021 enhancing tumor, had slightly lower performance. Dice scores generally plateaued at ~ 200 training samples, but sensitivity and F1 scores did continue to improve minimally with larger sample sizes. Finally, we found that the nnU-Net yielded slightly higher Dice scores relative to the reference standard than was found between the segmentations of the two radiologists (median

0.89 vs 0.86) and much better than prior work (0.75 (8)), but slightly lower sensitivity than radiologists (83% vs 86%).

Data Availability

Training data, consisting of 461 MRIs and annotations is available to download under a non-commercial license at <https://imagingdatasets.ucsf.edu/dataset/1>. Data from the 99 test subjects will become available after the completion of the 2023 MICCAI (Medical Image and Computing and Computer Assisted Intervention Society) challenge.

Discussion

The assessment of brain metastases represents an ideal use case for the translation of artificial intelligence methods into clinical practice. Data sharing efforts and competitions such as those by BraTS and RSNA have been critical for the advancement of biomedical image segmentation tasks as they provide large amounts of annotated data and a performance benchmark. Currently only one other public database of annotated brain metastases (n=105) exists <https://aimi.stanford.edu/brainmetshare> (6). Larger sample sizes with more heterogeneous data should allow for improved algorithm performance and generalizability, particularly for difficult to detect small metastases, as well as a clearer comparison of different algorithms.

While performance using the nnU-net was at the level of inter-rater reliability for Dice scores and better than prior networks (8), sensitivity was still lower. Given that sensitivity continued to improve with larger sample sizes, it is likely that even larger samples through additional data sharing efforts, or perhaps more novel network architectures/loss functions should allow for continued performance gains. This will be critical in helping lead to clinical implementation of automated brain metastasis segmentation algorithms.

The integration of artificial intelligence tools into clinical workflows should allow for more rapid and precise quantitative assessments of disease burden, ultimately enabling more accurate and efficient diagnosis and treatment. The evaluation and treatment of brain metastases represents an excellent use case for which more public data is needed. We hope that releasing this dataset will lead to the development of algorithms with better segmentation performance and ultimately improved care of patients with intracranial metastatic disease.

References

1. Clark K, Vendt B, Smith K, et al. The Cancer Imaging Archive (TCIA): maintaining and operating a public information repository. *J Digit Imaging*. United States: Mallinckrodt Institute of Radiology, Washington University School of Medicine, ERL 510 South Kingshighway Boulevard, St. Louis, MO, 63110, USA, clarkk\@mir.wustl.edu.; 2013;26(6):1045–1057. doi: 10.1007/s10278-013-9622-7.
2. Baid U, Ghodasara S, Bilello M, et al. The RSNA-ASNR-MICCAI BraTS 2021 Benchmark on Brain Tumor Segmentation and Radiogenomic Classification. *ArXiv210702314 Cs*. 2021; <http://arxiv.org/abs/2107.02314>. Accessed July 11, 2021.
3. Ostrom QT, Wright CH, Barnholtz-Sloan JS. Brain metastases: epidemiology. *Handb Clin Neurol*. Netherlands: Case Comprehensive Cancer Center, Case Western Reserve University School of Medicine, Cleveland, OH, United States.; 2018;149:27–42. doi: 10.1016/B978-0-12-811161-1.00002-5.
4. Arvold ND, Lee EQ, Mehta MP, et al. Updates in the management of brain metastases. *Neuro Oncol*. England: St. Luke's Radiation Oncology Associates, St. Luke's Cancer Center, Whiteside Institute for Clinical Research and University of Minnesota Duluth, Duluth, Minnesota (N.D.A.); Center for Neuro-Oncology, Dana-Farber/Brigham & Women's Cancer Center, Boston, Massachusetts (E.Q.L., P.Y.W.); Harvard Medical School, Boston, Massachusetts (E.Q.L., B.M.A., N.U.L., I.F.D., P.Y.W.); Department of Radiation Oncology, University of Maryland Medical Center, Baltimore, Maryland (M.P.M.); Department of Medical Oncology, City of Hope, Duarte, California (K.M.); Department of Radiation Oncology, Dana-Farber/Brigham & Women's Cancer Center, Boston, Massachusetts (B.M.A.); Department of Medical Oncology, Dana-Farber Cancer Institute, Boston, Massachusetts (N.U.L.); Department of Medicine, Division of Hematology-Oncology, University of North Carolina, Chapel Hill, North Carolina (C.K.A.); Department of Neurology/Neuro-Oncology, University of Turin, Turin, Italy (R.S.); Division of Medical Oncology, University of Colorado Denver, Denver, Colorado (D.R.C.); Department of Neurosurgery, Cleveland Clinic, Cleveland, Ohio (M.A.V.); Department of Neurosurgery, Brigham & Women's Hospital, Boston, Massachusetts (I.F.D.); 2016;18(8):1043–1065. doi: 10.1093/neuonc/nov127.
5. Mills SJ, Radon MR, Baird RD, et al. Utilization of volumetric magnetic resonance imaging for baseline and surveillance imaging in Neuro-oncology. *Br J Radiol*. England: 1 Department of Neuroradiology, The Walton Centre NHS Foundation Trust, Liverpool, United Kingdom.; 2019;92(1098):20190059. doi: 10.1259/bjr.20190059.
6. Grøvik E, Yi D, Iv M, Tong E, Rubin D, Zaharchuk G. Deep learning enables automatic detection and segmentation of brain metastases on multisequence MRI. *J Magn Reson Imaging*. United States: Department of Radiology, Stanford University, Stanford, California, USA.; 2020;51(1):175–182. doi: 10.1002/jmri.26766.

7. Bousabarah K, Ruge M, Brand J-S, et al. Deep convolutional neural networks for automated segmentation of brain metastases trained on clinical data. *Radiat Oncol Lond Engl*. 2020;15. doi: 10.1186/s13014-020-01514-6.
8. Rudie JD, Weiss DA, Colby JB, et al. Three-dimensional U-Net Convolutional Neural Network for Detection and Segmentation of Intracranial Metastases. *Radiology: Artificial Intelligence*. 2021;3(3):e200204. doi: 10.1148/ryai.2021200204.
9. Isensee F, Jaeger PF, Kohl SAA, Petersen J, Maier-Hein KH. nnU-Net: a self-configuring method for deep learning-based biomedical image segmentation. *Nat Methods*. Nature Publishing Group; 2020;1–9. doi: 10.1038/s41592-020-01008-z.
10. Yushkevich PA, Piven J, Hazlett HC, et al. User-guided 3D active contour segmentation of anatomical structures: Significantly improved efficiency and reliability. *NeuroImage*. 2006;31(3):1116–1128. doi: 10.1016/j.neuroimage.2006.01.015.
11. Luu HM, Park S-H. Extending nn-UNet for brain tumor segmentation. *ArXiv211204653 Cs Eess*. 2021; <http://arxiv.org/abs/2112.04653>. Accessed January 29, 2022.

Tables

Table 1. Patient Demographics, Cancer Types and Metastases Statistics

	Total
Demographics	
Number of Patients	412
Number of MRIs	560
Age (Mean +/- SD)	61 +/- 12
Men:Women	174:238
Primary Cancer Types	
Lung	172
Breast	96
Melanoma	52
Renal	22
Head and Neck	11
Other Genitourinary	10
Other Gastrointestinal	9
Rectal	8
Neuroendocrine	5
Colon	6
Prostate	10
Thyroid	4
Other/Unknown	7
Metastases Information	
Prior Craniotomy/Resection/Biopsy:No Prior Surgery	135:425
Total Number of Metastases	5136
Number of Metastasis (mean ± SD, median (25-75 IQR))	9.2 ± 12.9, 5 (2-10)
Total Metastases Volume (cm ³ ; mean ± SD, median (25-75 IQR))	5.3 ± 6.9, 2.6 (0.6-6.9)
Individual Metastasis Volume (cm ³ ; mean ± SD, median (25-75 IQR))	0.57 ± 2.1, 0.05 (0.02-0.18)

Note.— Continuous variables are shown as average ± standard deviation (SD) or median (interquartile range [IQR]).

Table 2. nnU-Net Segmentation Performance Metrics

Experiment	Dice		Overall Detection Performance			Average Detection Performance		
	Mean +/- SD	Median (25-75 IQR)	Sensitivity	Precision	F1 score	Sensitivity	Precision	F1 score
Different Inputs								
T1-post	0.84 ± 0.12	0.88 (0.82-0.91)	81.92%	91.77%	0.87	88.2 ± 17.7%	93.6 ± 14.3%	0.87 ± 0.19
Subtraction	0.85 ± 0.14	0.89 (0.83-0.92)	78.67%	89.41%	0.84	86.9 ± 20.9%	89.8 ± 19.3%	0.85 ± 0.21
T1 and T1-post	0.86 ± 0.11	0.89 (0.84-0.92)	81.21%	92.74%	0.87	88.3 ± 17.2%	94.1 ± 13.3%	0.88 ± 0.18
<i>T1, T1-post, and Subtraction</i>	<i>0.86 ± 0.11</i>	<i>0.89 (0.85-0.92)</i>	<i>82.91%</i>	<i>93.17%</i>	<i>0.88</i>	<i>89.3 ± 17.0%</i>	<i>94.8 ± 13.4%</i>	<i>0.88 ± 0.19</i>
T1, T1-post, and FLAIR	0.86 ± 0.10	0.89 (0.84-0.91)	80.79%	93.77%	0.87	88.4 ± 18.0%	95.1 ± 12.7%	0.88 ± 0.19
T1, T1-post, Subtraction, and FLAIR	0.86 ± 0.10	0.89 (0.85-0.92)	81.36%	93.35%	0.87	88.9 ± 17.2%	95.1 ± 11.7%	0.88 ± 0.18
Different Network Configurations								
Batch Size = 6	0.85 ± 0.11	0.89 (0.84-0.92)	81.21%	95.36%	0.88	87.0 ± 19.2%	96.4 ± 10.9%	0.88 ± 0.19
Five-Fold Cross Validation	0.86 ± 0.11	0.89 (0.84-0.92)	81.07%	93.49%	0.87	88.1 ± 18.2%	94.9 ± 13.9%	0.88 ± 0.19
Pre-trained on BraTS 2021	0.84 ± 0.12	0.87 (0.81-0.91)	76.13%	93.58%	0.84	84.4 ± 21.9%	94.0 ± 17.1%	0.86 ± 0.20
Luu et al., 2021 Configuration	0.85 ± 0.13	0.89 (0.84-0.92)	81.78%	94.76%	0.88	88.9 ± 17.3%	95.8 ± 12.2%	0.89 ± 0.18
Smaller Train Sample Sizes								
n=10	0.72 ± 0.22	0.79 (0.65-0.87)	60.03%	97.25%	0.74	73.5 ± 28.0%	95.6 ± 16.6%	0.80 ± 0.23
n=25	0.76 ± 0.21	0.84 (0.71-0.90)	61.72%	97.98%	0.76	74.5 ± 28.4%	96.1 ± 15.8%	0.81 ± 0.23
n=50	0.82 ± 0.15	0.86 (0.79-0.90)	67.37%	97.15%	0.80	78.8 ± 25.8%	95.9 ± 14.5%	0.83 ± 0.22
n=75	0.82 ± 0.16	0.87 (0.80-0.90)	73.59%	95.42%	0.83	82.3 ± 23.1%	95.4 ± 15.2%	0.86 ± 0.20
n=100	0.82 ± 0.16	0.88 (0.79-0.91)	74.44%	92.62%	0.83	82.6 ± 22.8%	93.2 ± 18.4%	0.85 ± 0.21
n=150	0.83 ± 0.15	0.87 (0.81-0.91)	74.15%	94.59%	0.83	82.7 ± 22.9%	94.1 ± 17.6%	0.84 ± 0.20
n=200	0.84 ± 0.15	0.88 (0.81-0.92)	78.11%	95.34%	0.86	86.3 ± 19.4%	96.3 ± 11.0%	0.88 ± 0.19
n=300	0.85 ± 0.12	0.89 (0.84-0.92)	80.93%	93.17%	0.87	87.7 ± 19.0%	94.5 ± 13.3%	0.87 ± 0.19
n=400	0.85 ± 0.12	0.89 (0.84-0.92)	81.64%	93.08%	0.87	88.7 ± 21.9%	93.8 ± 13.4%	0.88 ± 0.19
Human Inter-Rater Performance								
Radiologist 1 vs Radiologist 2	0.83 ± 0.09	0.86 (0.80-0.89)	86.71%	85.36%	0.86	90.7 ± 15.7%	88.5 ± 21.2%	0.87 ± 0.19
Radiologist 2 vs Radiologist 1	0.83 ± 0.09	0.86 (0.80-0.89)	84.68%	87.87%	0.86	89.8 ± 17.9%	89.4 ± 20.0%	0.87 ± 0.20
Radiologist 1 vs Gold Standard	0.90 ± 0.06	0.91 (0.89-0.94)	85.59%	97.15%	0.92	90.4 ± 16.8%	97.9 ± 14.4%	0.92 ± 0.17
Radiologist 2 vs Gold Standard	0.94 ± 0.06	0.96 (0.93-0.98)	88.56%	95.42%	0.94	92.0 ± 14.2%	97.9 ± 14.4%	0.93 ± 0.16

Note.— Continuous variables are shown as average ± standard deviation (SD) or median (interquartile range [IQR]).

Figures

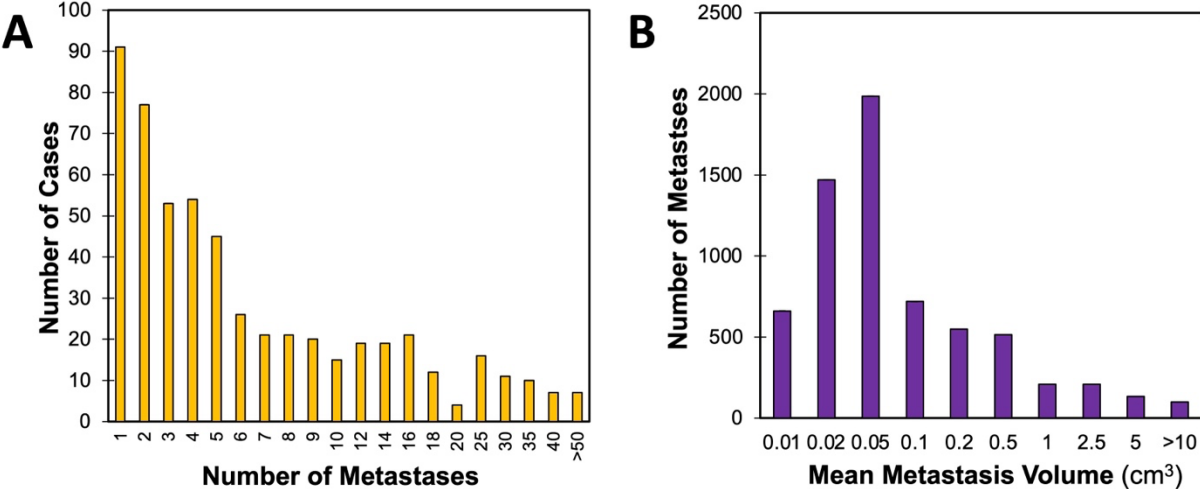


Figure 1. Distribution of number and size of brain metastases. Counts of number of manually segmented brain metastases per MRI (a) and average brain metastasis volume (b).

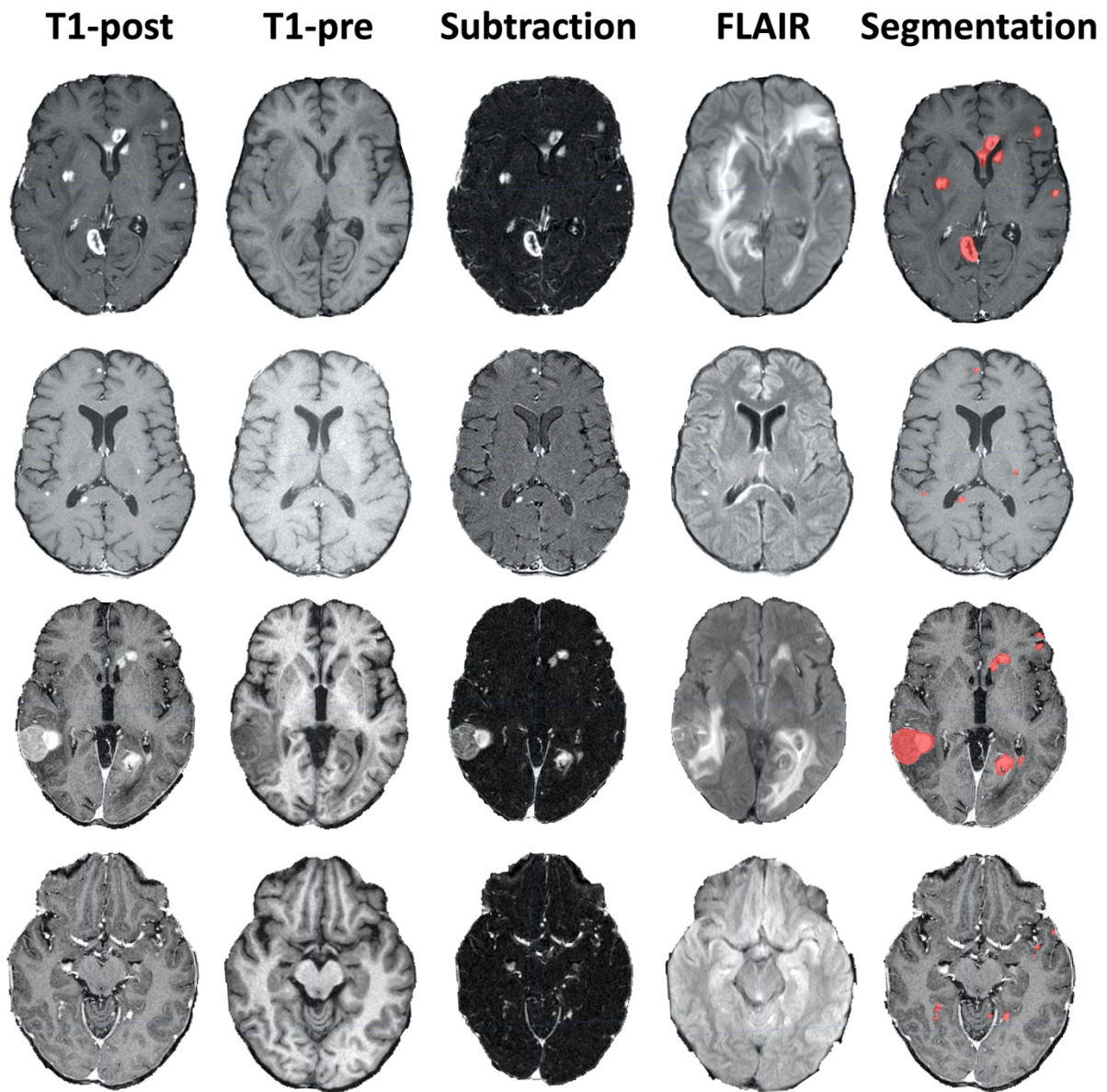


Figure 2. Example Brain Metastases Data. Four example MRIs with axial T1 post-contrast images (T1-post), T1 pre-contrast images (T1-pre), subtraction images, FLAIR images, and ground truth segmentations overlaid on the T1 post-contrast images.